Eur. Phys. J. Spec. Top.
https://doi.org/10.1140/epjs/s11734-024-01177-4

THE EUROPEAN PHYSICAL JOURNAL SPECIAL TOPICS

Review

Mesoscopic modeling of membranes at cellular scale

Anil K. Dasanna[1,2,a] and Dmitry A. Fedosov[3,b]

[1] Department of Physics, Indian Institute of Technology, Palakkad 678623, India
[2] Department of Physical Sciences, Indian Institute of Science Education and Research (IISER) Mohali, Sector 81, Knowledge City, Mohali 140306, India
[3] Theoretical Physics of Living Matter, Institute for Advanced Simulation, Forschungszentrum Jülich, 52425 Jülich, Germany

Received 12 December 2023 / Accepted 23 April 2024

Abstract Cellular membranes span a wide range of spatio-temporal scales from sub-microsecond dynamics of lipid molecules and intra-membrane proteins to multi-minute deformations of the whole cell. Since no single simulation method would cover all these scales, there exists a variety of membrane modeling techniques, each presenting unique advantages for addressing a diverse range of scientific questions. This review focuses on current advances in mesoscopic models that represent membranes as two-dimensional surfaces with selected mechanical properties. Two categories of approaches are considered, including fluid membrane (e.g., lipid bilayer) and polymerized membrane (e.g., red blood cell) models. Both particle-based and continuum models for these two classes of membranes are discussed. To illustrate the potential of these models, several examples from recent simulation studies are presented, including equilibrium and non-equilibrium membrane structures, membrane remodeling, and deformation in fluid flow. Finally, we briefly discuss further developments related to these membrane models.

1 Introduction

Membranes are key components of every biological cell, since they serve as physical boundaries between different organelles inside the cell, internal cell compartments, and cells within a tissue, and play a crucial role in a variety of biological processes [1]. Therefore, understanding the behavior and properties of cellular membranes is essential for gaining insights into cellular functions, such as signal transduction [2, 3], cell morphology [4, 5], and motility [6, 7]. Biological membranes primarily consist of phospholipid molecules, with a variety of embedded proteins (e.g., membrane channels, receptors) [8, 9]. There also exist a variety of synthetic membranes made of polymeric materials such as block copolymers, dendrimers, etc. [10–12]. Despite significant advances in microscopy techniques during the last decade, which often allow detailed observations of the behavior of biological and artificial membranes, theoretical and computational approaches remain as important tools for studying membranes to complement experiments or go even beyond experimental capabilities [13–19].

The field of membrane modeling includes a diverse range of simulation techniques [13–17, 20], each offering distinct advantages for addressing specific scientific questions. At the atomistic level [15, 21–26], molecular dynamics simulations provide a detailed representation of atomic structure of individual lipid molecules, such that a relatively small membrane patch ($\sim \mu m^2$) over short time scales ($\sim \mu s$) can be simulated. Simulations of larger length and time scales with atomistic resolution are still substantially limited by rapidly growing computational costs. To overcome this limitation, coarse-grained models of membranes have emerged, where individual lipids are represented by a few particles [27–33]. Coarse-grained models of membranes are computationally cheaper than the atomistic models, but they partially or fully lose molecular specificity. The next level of abstraction going away from the molecular description corresponds to models, which represent membranes as two-dimensional (2D) surfaces with specific mechanical properties such as bending rigidity, shear elasticity, and the resistance to area dilation [34–41]. This class of simulation techniques includes meshless membrane models [34, 36, 42–45], triangulated network approaches [35, 37, 41, 46–50], and continuum models [38–40, 51–54].

[a] e-mail: adasanna@iisermohali.ac.in (corresponding author)
[b] e-mail: d.fedosov@fz-juelich.de

Published online: 07 May 2024

In this review, we focus on the approaches that represent membranes as 2D surfaces [34–41]. These techniques allow modeling of membranes at the cellular scale, enabling simulations of single cells or vesicles as well as multicellular suspensions [13, 14, 55–58]. Specifically, we consider two distinct classes of membranes: (i) fluid membranes and (ii) polymerized membranes. Examples of fluid membranes include lipid bilayers and some polymer-based membranes [8, 10–12]. Fluid membranes can flow, such that they allow the motion of intra-membrane inclusions (e.g., lipids, proteins) and can be thought of as 2D fluidic surfaces [59, 60]. The main mechanical properties of fluid membranes can be characterized by the bending rigidity, membrane viscosity, and nearly zero area dilation [27, 32, 61–63]. In contrast, polymerized membranes generally contain a cross-linked network of proteins or polymers, with examples of a cytoskeletal network supporting lipid bilayer in the cell [62, 64, 65] and synthetic capsules [66–68]. Thus, polymerized membranes are elastic and possess a non-zero shear elasticity [69, 70], in addition to the bending rigidity and the resistance to area dilation.

We present several mesoscopic models of fluid and polymerized membranes, and illustrate them using a selection of recent applications. For fluid membranes, we discuss examples of active vesicles [71–80], protein-driven vesicle fission [81–86], and membrane shape remodeling through curvature-inducing proteins [87–96]. For polymerized membranes, we focus on red blood cells (RBCs), and discuss membrane fluctuations [97–107], deformation of RBCs in flow [108–124], and the adhesion of malaria parasite to RBCs [125–132]. These examples illustrate that the existing methods for membrane modeling are quite mature, and have a wide range of the applicability to a variety of cellular-scale problems.

2 Fluid membrane models

Fluid membranes are represented by fluidic 2D surfaces with a non-zero bending rigidity. Different simulation approaches include dynamically triangulated membrane models [35, 46, 133–136], meshless membrane models [34, 36, 42–45], and continuum models [51, 52, 137–141].

2.1 Dynamically triangulated membrane model

A fluid membrane can be modeled by a dynamically triangulated network of N_v linked vertices [46, 133]. The links are represented by a tethering potential [46, 78, 142] as

$$U_\mathrm{att}(r) = \begin{cases} k_\mathrm{b} \frac{\exp\left[1/(l_{c_0}-r)\right]}{l_\mathrm{max}-r} & \text{if } r > l_{c_0} \\ 0 & \text{if } r \le l_{c_0} \end{cases}, \tag{1}$$

$$U_\mathrm{rep}(r) = \begin{cases} k_\mathrm{b} \frac{\exp\left[1/(r-l_{c_1})\right]}{r-l_\mathrm{min}} & \text{if } r < l_{c_1} \\ 0 & \text{if } r \ge l_{c_1} \end{cases}, \tag{2}$$

where k_b is the bond stiffness, l_min and l_max are the minimum and maximum bond lengths, and l_{c_1} and l_{c_0} are the potential cutoff lengths. Thus, membrane vertices can move freely in the range $[l_{c_1}, l_{c_0}]$.

Bending elasticity is represented by the Helfrich curvature energy [61, 63, 143] as

$$U_\mathrm{bend} = 2\kappa_\mathrm{c} \oint_A (\bar{c} - c_0)^2 \mathrm{d}A + \kappa_\mathrm{k} \oint_A K \mathrm{d}A, \tag{3}$$

where κ_c is the bending modulus, $\bar{c} = (c_1 + c_2)/2$ is the local mean curvature, c_0 is the spontaneous curvature, A is the total membrane area, κ_k is the Gaussian (or saddle splay) modulus, and $K = c_1 c_2$ is the Gaussian curvature. Note that the surface integral over the Gaussian curvature K is constant for closed surfaces (e.g., vesicle) due to the Gauss–Bonnet theorem [144], so that the Gaussian term in Eq. (3) is often neglected in simulations. The bending energy without the Gaussian curvature contribution is discretized on a triangulated network [35, 145] as

$$U_\mathrm{bend} = \sum_{i=1}^{N_\mathrm{v}} \frac{2\kappa_\mathrm{c}(\bar{c}_i - c_{0_i})^2 A}{N_\mathrm{v}} = 2\kappa_\mathrm{c} \sum_{i=1}^{N_\mathrm{v}} \sigma_i \left[\frac{1}{2\sigma_i} \mathbf{n}_i \cdot \left(\sum_{j(i)} \frac{\sigma_{ij}}{r_{ij}} \mathbf{r}_{ij} \right) - c_{0_i} \right]^2, \tag{4}$$

where $\bar{c}_i$ and c_{0_i} are the mean and spontaneous curvatures at vertex i with an area A/N_v, $\mathbf{n}_i$ is a unit normal of the membrane at vertex i, and $\sigma_i = \left(\sum_{j(i)} \sigma_{ij} r_{ij}\right)/4$ is the area of dual cell of vertex i. $j(i)$ stands for all neighboring vertices linked to the vertex i, $\sigma_{ij} = r_{ij}[\cot(\theta_1) + \cot(\theta_2)]/2$ is the length of the bond in dual lattice with angles

θ_1 and θ_2 being the two angles opposite to the shared bond vector $\mathbf{r}_{ij}$. More details about discretization of the Helfrich curvature energy, including other discretization strategies, can be found in Refs. [46, 145–151].

Furthermore, local triangle area conservation is imposed by a soft harmonic potential given by

$$U_{\text{loc. area}} = \frac{k_{\text{l}}}{2} \sum_{i=1}^{N_{\text{t}}} \frac{(A_i - A')^2}{A'}, \tag{5}$$

where k_{l}, $A' = A/N_{\text{t}}$, and A_i are the local-area conservation coefficient, desired and instantaneous local areas, respectively. The sum runs over all $N_{\text{t}} = 2(N_{\text{v}} - 2)$ triangles within the network. When necessary, a constraint on the total vesicle volume V can be employed as

$$U_{\text{vol}} = \frac{k_{\text{v}}(V - V_0)^2}{2V_0}, \tag{6}$$

where k_{v} is the volume-constraint coefficient and V_0 is the desired total volume.

The membrane model with a fixed network connectivity cannot represent membrane fluidity where its vertices diffuse within the membrane plane. To model membrane fluidity, bonds shared by each pair of triangles are flipped. The flipping procedure is performed with a time frequency ν, i.e., every few time steps. During the flipping procedure, every bond in the membrane network is attempted to be flipped with a probability ψ, where the acceptance of bond flipping follows a Monte-Carlo algorithm. In the Monte-Carlo algorithm, changes in the tethering (i.e., $\Delta U_{\text{att}} + \Delta U_{\text{rep}}$) and local area (i.e., $\Delta U_{\text{loc. area}}$) energies due to attempted bond flipping are computed, and the bond flipping is accepted with a probability $\exp\left[-(\Delta U_{\text{att}} + \Delta U_{\text{rep}} + \Delta U_{\text{loc. area}})/k_B T\right]$. Note that a change in the bending energy is often omitted due to simplicity, as bond flipping has a negligible effect on the local membrane curvature. The resulting membrane fluidity for selected parameters ν and ψ can be characterized by a 2D membrane viscosity, see Refs. [142, 152] for details.

2.2 Meshless membrane model

Another fluid membrane model is the one-particle-thick meshless membrane model [45]. In this model, a membrane consists of a collection of particles with position vectors $\mathbf{r}_i$ and orientation vectors $\mathbf{n}_i$, which are subject to pairwise interactions. The interaction potential for a pair of membrane particles i and j is given by [45]

$$U(\mathbf{r}_{ij}, \mathbf{n}_i, \mathbf{n}_j) = \begin{cases} u_R(r) + [1 - \phi(\hat{\mathbf{r}}_{ij}, \mathbf{n}_i, \mathbf{n}_j)]\varepsilon, & r < r_{min}, \\ u_A(r)\phi(\hat{\mathbf{r}}_{ij}, \mathbf{n}_i, \mathbf{n}_j) & r_{min} < r < r_c, \end{cases} \tag{7}$$

where $\mathbf{r}_{ij} = \mathbf{r}_i - \mathbf{r}_j$, $r = |\mathbf{r}_{ij}|$, and $\hat{\mathbf{r}}_{ij} = \mathbf{r}_{ij}/r$. The repulsive ($u_R$) and attractive ($u_A$) potentials are defined as

$$u_R(r) = \varepsilon\left[\left(\frac{r_{min}}{r}\right)^4 - 2\left(\frac{r_{min}}{r}\right)^2\right],\ u_A(r) = -\varepsilon\left[\cos\left(\frac{\pi}{2}\frac{(r - r_{min})}{(r_c - r_{min})}\right)\right]^{2\zeta}, \tag{8}$$

where ε is the strength of the potentials, r_{min} is the cutoff of repulsive forces, r_c is the total cutoff of interactions, and ζ is an exponent. The interaction strength $\phi(\hat{\mathbf{r}}_{ij}, \mathbf{n}_i, \mathbf{n}_j)$ for different relative orientations is given by

$$\phi(\hat{\mathbf{r}}_{ij}, \mathbf{n}_i, \mathbf{n}_j) = 1 + \mu[a(\hat{\mathbf{r}}_{ij}, \mathbf{n}_i, \mathbf{n}_j) - 1], \tag{9}$$

$$a(\hat{\mathbf{r}}_{ij}, \mathbf{n}_i, \mathbf{n}_j) = (\mathbf{n}_i \times \hat{\mathbf{r}}_{ij}) \cdot (\mathbf{n}_j \times \hat{\mathbf{r}}_{ij}) + \sin(\theta_0)(\mathbf{n}_j - \mathbf{n}_i) \cdot \hat{\mathbf{r}}_{ij} - \sin^2(\theta_0), \tag{10}$$

where θ_0 determines spontaneous angle between two particle orientations, and μ weighs the energy penalty when the angle between two particle orientations departs from θ_0.

Particle positions are integrated using the Langevin equation (14), while the time evolution of particle orientations follows the Lagrange equations with constraint forces,

$$I_i \ddot{\mathbf{n}}_i = -\frac{\partial U_i}{\partial \mathbf{n}_i} + \lambda_i \mathbf{n}_i, \quad \lambda_i = \frac{\partial U_i}{\partial \mathbf{n}_i} \cdot \mathbf{n}_i - I_i \dot{\mathbf{n}}_i \cdot \dot{\mathbf{n}}_i, \tag{11}$$

where I_i is the moment of inertia, $U_i = \sum_j U(\mathbf{r}_{ij}, \mathbf{n}_i, \mathbf{n}_j)$, and λ_i is the Lagrange multiplier.

There also exist other meshless models of membranes [34, 36, 42–44]. The model in Ref. [43] has considered dipole-like interactions between oriented particles in order to support their sheet-like assembly. In Ref. [36], moving

least-squares method was used to implement the curvature energy in the membrane model. One of the main advantages of meshless membrane models in comparison to dynamically triangulated network models is the ability of spontaneous membrane break-up (e.g., vesicle fission, budding), which does not require additional conditions and assumptions. For dynamically triangulated networks, break-up conditions have to be defined to maintain the proper triangulation of newly formed membrane components.

2.3 Continuum models of fluid membranes

Continuum models of fluid vesicles also employ the Helfrich bending energy [61, 63, 143] in Eq. (3). One of the common procedures is to apply a variational formulation, in which a variational derivative of Eq. (3) is taken to derive membrane forces [148, 149]. If $\delta\boldsymbol{x}$ is a small virtual displacement of a surface, the work performed by the forces is given by $\Delta\boldsymbol{f}_b \cdot \delta\boldsymbol{x}$. For the whole membrane, the work from external forces is obtained as

$$\delta W_e = \int_A \Delta\boldsymbol{f}_b \cdot \delta\boldsymbol{x} \mathrm{d}A. \tag{12}$$

In equilibrium, the change in energy should vanish such that $\delta U = \delta U_{\mathrm{bend}} - \delta W_e = 0$. The evaluation of δU_{bend} results in the Euler–Lagrange equation [120, 144, 163]

$$\Delta\boldsymbol{f}_b = -2\kappa_c\big[\Delta_A(\bar{c} - c_0) + 2(\bar{c} - c_0)(\bar{c}^2 - K + c_0\bar{c})\big]\boldsymbol{n}, \tag{13}$$

where Δ_A is the Laplace–Beltrami operator [144], and $\boldsymbol{n}$ is the normal to the surface. Then, an equilibrium shape of a membrane can be found for $\Delta\boldsymbol{f}_b = 0$. For hydrodynamic simulations, $\Delta\boldsymbol{f}_b$ is defined by instantaneous deformation through the forces exerted by the fluid on the membrane. Other methods employ thin shell theory [140, 164, 165] to derive the Euler–Lagrange equation by computing derivatives of the energy density with respect to metric and curvature tensors. However, these formulations lead to the same results [149, 164]. Other constraints (e.g., area and volume conservation) can be included through additional terms to U using Lagrange multipliers, which modify the Euler–Lagrange equation. For example, the total surface area constraint can be implemented by adding $\sigma \int_A dA$ to U with the Lagrange multiplier σ, representing effective membrane tension [144, 149, 151, 164].

2.4 Comparison of different models

There exist differences between different models; however, when used properly, they should lead to the same results, because only physical properties of membranes should govern their behavior. In this respect, advantages/disadvantages of different models can be rather subtle, and generally appear at the computational and algorithmic levels, representing for instance numerical accuracy, ease of implementation and parallelization, and computational cost. As an example, the dynamically triangulated model implements membrane fluidity by flipping the bonds. As a result, the viscosity of the membrane is controlled by the frequency of bond flips, which has an upper limit, so that this model may have difficulties to represent low membrane viscosities. In contrast, the meshless membrane model naturally incorporates membrane fluidity as its particles are not connected by bonds and interact via only pair potentials. However, the meshless model is likely computationally expensive for situations, where a large membrane viscosity is required, since strong dissipative interactions between the particles would be required. Another drawback of the meshless membrane model is that the implementation of membrane volume conservation is more difficult than for the dynamically triangulated model.

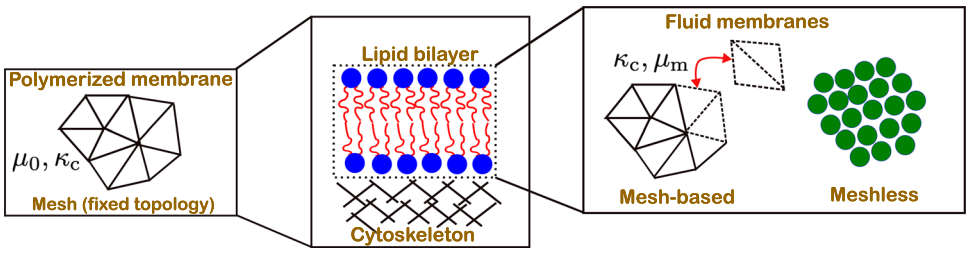

Fig. 1 A sketch summarizing fluid and polymerized membrane models. A fluid membrane (e.g., lipid bilayer) can be modeled using dynamically triangulated surface with bond flips that introduce fluidity and by the meshless model. The fluid membrane is characterized by the bending rigidity κ_c and membrane viscosity μ_{m}. The triangulated membrane model with a fixed bond topology represents a polymerized membrane (e.g., lipid bilayer with a cytoskeleton beneath it). The polymerized membrane is characterized by the shear modulus μ_0 as well as by κ_c and μ_{m} for fluid membranes

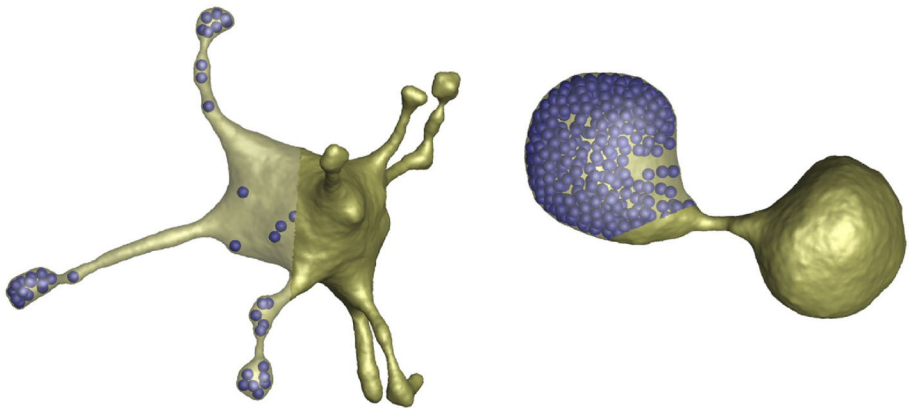

Fig. 2 3D simulations of vesicles enclosing active particles [71, 78]. (Left) A low volume fraction of active particles generally leads to multiple tether-like protrusions, resembling an astrocyte-like shape. (Right) A large volume fraction of self-propelled particles induces global shape changes, which may resemble cell division

Differences between the models are partially summarized in Fig. 1, which illustrates fluid and polymerized membrane models. Both the dynamically triangulated model with bond flips and the meshless model represent fluid membranes, while a triangulated surface model with a fixed bond topology represents a membrane with a non-zero elasticity (e.g., a RBC membrane which contains a cytoskeleton). Nevertheless, different models can also share some physical characteristics, for instance, the bending rigidity which is generally required for both fluid and polymerized membranes.

A comparison of continuum and particle-based models can also be quite subtle. Continuum models generally represent homogeneous physical characteristics of membranes, while particle-based models may have local variations in physical properties due to the discrete nature of membrane representation. Computational cost of different models is difficult to compare, as it depends on the problem of interest and the method of implementation.

All membrane models can be integrated in time using several approaches. The simplest approach is Monte-Carlo modeling, which aims at energy minimization of the system of interest, but cannot properly capture the dynamics of this system. Without hydrodynamic interactions, dynamics of membranes can be modeled by the Langevin equation,

$$m\ddot{\mathbf{r}}_i = -\nabla_i U_{\text{tot}} - \gamma_{\text{m}}\dot{\mathbf{r}}_i + \sqrt{2\gamma_{\text{m}}k_{\text{B}}T}\boldsymbol{\xi}_i(t), \tag{14}$$

where m is the particle mass, ∇_i is the spatial derivative at the position of particle i, and U_{tot} is the sum of all interaction potentials. The friction coefficient γ_{m} mimics embedding of the membrane into a viscous fluid through the free-draining approximation. $\boldsymbol{\xi}_i(t)$ is a Gaussian random process with $\langle\boldsymbol{\xi}_i(t)\rangle = \mathbf{0}$ and $\langle\boldsymbol{\xi}_i(t)\boldsymbol{\xi}_j(t')\rangle = \mathbf{1}\delta_{ij}\delta(t-t')$ that represents membrane thermal fluctuations. The positions and velocities of all particles are integrated using the velocity-Verlet algorithm [153].

When hydrodynamic interactions are necessary, the membrane model has to be coupled to a fluid. The fluid can be modeled through a variety of different methods, which is beyond the scope of this review, but we refer an interested reader to Refs. [154–159]. Coupling between the membrane and the fluid is often performed using the immerse boundary method [160, 161], where the membrane discretization points move with the local fluid velocity, and in response exert forces onto the fluid. Another way to implement this coupling is to introduce frictional forces between the membrane and the fluid, which imposes the exchange of momentum between the membrane and fluid models [41, 162].

3 Fluid membrane applications

3.1 Active vesicles

Bottom-up construction of synthetic cell-mimicking systems has made an enormous progress in recent years [166, 167]. Examples include vesicles with enclosed active particles [71–80], and growth and spontaneous division of droplet-based or vesicle-based compartments [94, 168]. The main advantage of bottom-up synthetic systems is a precise control of their composition, which allows to study different cell-mimicking processes in much simpler systems in comparison to biological cells. Numerical simulations provide here a more detailed and controlled representation of synthetic systems, leading to the understanding of their behavior [71, 73–79].

The behavior of an active vesicle system (see Fig. 2), where self-propelled particles (SPPs) are encapsulated inside the vesicle and interact with the membrane through a purely repulsive potential, was studied in Refs. [71, 78]. The vesicle was modeled using the dynamically triangulated membrane model, see Sect. 2.1. This active

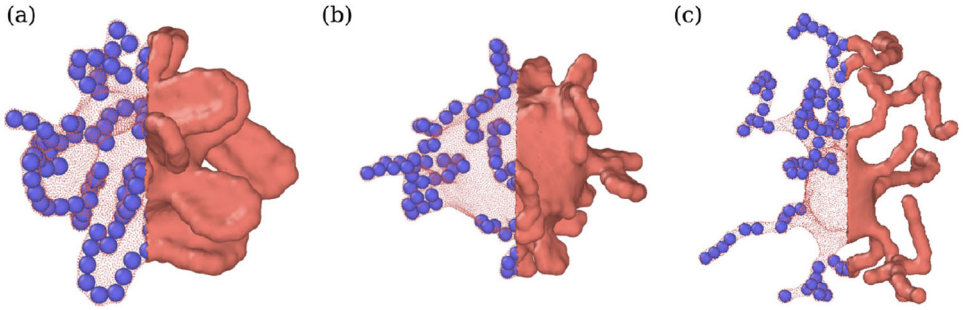

Fig. 3 Vesicle shapes for different SPP propulsion strengths and moderate adhesive interactions. Particle structures change from membrane-wrapped ring-like arrangements to membrane-wrapped (branched) tubular aggregates, as the propulsion force is increased. Reproduced from Ref. [79] with permission from the Royal Society of Chemistry

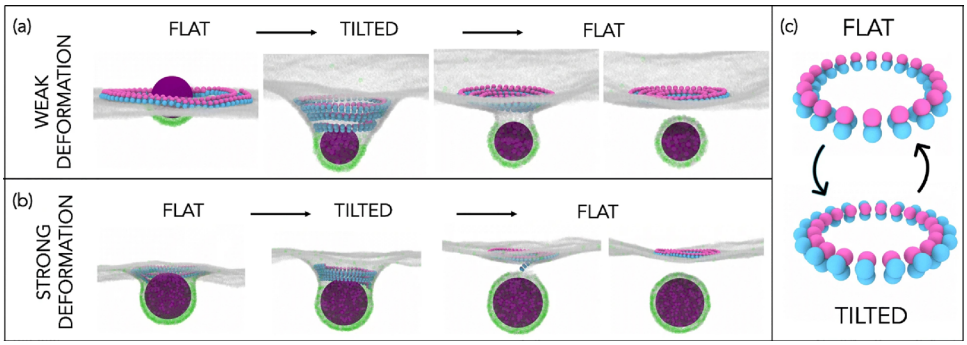

Fig. 4 Filament transitions from flat to tilted [see (**c**)] states and back drive membrane budding. (**a**, **b**) Budding off aided by the filament for weak and strong membrane deformations induced by different adhesion strengths. Reproduced from Ref. [82] with permission from Springer Nature

system exhibits a variety of dynamic non-equilibrium vesicle shapes, including bola-like shapes and structures with multiple tether-like protrusions formed by single SPPs or their clusters, depending on the volume fraction of enclosed SPPs and their propulsion strength. Furthermore, such active vesicles show strongly enhanced membrane fluctuations, which is a clear signature of this non-equilibrium system [71, 72]. Despite the fact that this system does not have an internal autonomous control, it can be thought of as a prototype of a cell-mimicking system or soft microrobot.

Repulsive interactions between the vesicle membrane and SPPs constrain active particles to remain within the vesicle. Already in this simple situation, most of the active particles are located near the membrane [71, 78]. This is due to a so-called wall accumulation effect, which is related to the time of particle re-orientation governed by its rotational diffusion [169–171]. Thus, after arriving at a wall with a direction toward the wall, a SPP requires some time to re-orient away from the wall to be able to leave it. In addition to repulsive interactions, there are many examples of particle-membrane attraction, which can result in partial wrapping of the particle by the membrane [172–179]. Particle wrapping by the membrane is expected to lower the force required for tether formation, since some fraction of elastic membrane-bending energy is already overcome through particle adhesion or attractive interactions. Furthermore, attractive particle–membrane interactions will likely affect cluster formation and the behavior of active vesicles.

The effect of particle–membrane interactions on the dynamics of active vesicles has been investigated for several attraction strengths, which induce slight attraction without significant wrapping, partial wrapping, and nearly full wrapping of the particle by the membrane [79]. At low SPP activity, adhesive interactions dominate over the propulsion forces, such that the vesicle attains near static configurations, with protrusions of membrane-wrapped SPPs having ring-like and sheet-like structures [see Fig. 3a]. At moderate particle densities and strong enough activities, active vesicles show dynamic highly branched tethers filled with string-like arrangements of SPPs [see Fig. 3c], which do not occur in the absence of particle adhesion to the membrane [71, 78]. At large volume fractions of SPPs, vesicles fluctuate for moderate particle activities, and elongate and finally split into two daughter vesicles for large SPP propulsion strengths. The adhesion of SPPs to the membrane significantly alters the behavior of active vesicles, and provides an additional parameter for controlling their behavior.

3.2 Vesicle fission driven by ESCRT-III proteins

The ESCRT-III (endosomal sorting complexes required for transport III) proteins can deform and cut membranes of cells from the inside [180, 181]. ESCRT-III form spiral filament structures (see Fig. 4) that interact attractively

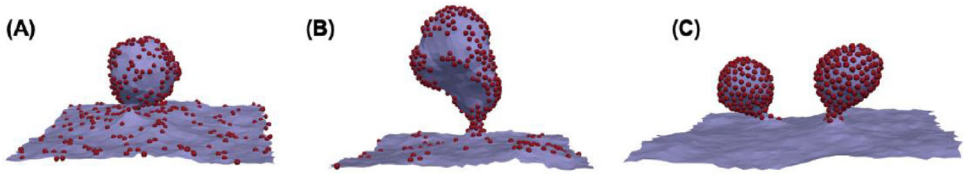

Fig. 5 Remodeling of a membrane by curvature-inducing proteins. Red vertices represent membrane inclusions, which induce a non-zero spontaneous curvature locally. The fraction of inclusions is 20%. From (**A**) to (**C**), the interaction strength between inclusions is increased, promoting their clustering. A high local concentration of inclusions leads to the formation of complex invaginations. Reproduced from Ref. [186]

with the membrane, and assist cells in division [181], membrane budding [81, 182], and the release of viral particles [183]. ESCRT-III filaments can form helices and cones, indicating that this protein may adapt to local conditions [184, 185]. In the model of Ref. [82], filaments can alternate between two geometrical states: (i) a ring flat (quasi-2D) geometry leading to the formation of a spiral structure when bound to a membrane, and (ii) a helical structure when bound to a tubular-like membrane surface. The membrane was modeled using the meshless membrane model described in Sect. 2.2. When the flat ESCRT-III state transits toward 3D helical structure, the protein is able to deform the membrane outwards from the inner side of the membrane, see Fig. 4. Interestingly, there is no significant difference in the action of ESCRT-III, depending on the degree of particle wrapping by the membrane. Figure 4 shows that particles with a weak adhesion (nearly no wrapping) and a strong adhesion (significant wrapping) receive qualitatively similar assistance by the ESCRT-III protein and eventually bud off. Therefore, the simulations suggest that filament transitions between these two states drive the budding process [82]. This model not only explains membrane remodeling observed in a number of biological systems, but also proposes possible ways of constructing active structures (e.g., self-assembled DNA origami) which would be able to remodel artificial membrane systems.

3.3 Membrane shape changes through curvature-inducing proteins

Curvature inducing proteins within the membrane or upon their adhesion can completely remodel membrane and vesicle shapes [87–96]. Figure 5 shows the remodelling of a membrane when the local concentration of curvature-inducing proteins (marked by red vertices) becomes large enough [186]. The membrane was modeled using the dynamically triangulated membrane model, see Sect. 2.1. The remodeling process can lead to the formation of buds and long tubular membrane structures, which appear due to the segregation of inclusions between the curved and flat membrane parts [88, 91, 92, 187]. Furthermore, local tension of the membrane can increase, affecting overall properties of the membrane [89, 188]. In addition to the local concentration of curvature-inducing proteins, the strength of local curvature they impose plays an essential role for the formation of complex membrane invaginations [91, 187]. The segregation or clustering of proteins occurs due to the coupling between local membrane geometry and the inclusion curvature, which results in attractive or repulsive membrane-mediated interactions between inclusions [189–191]. A similar effect has also been found for particles adhered to the membrane [178, 192, 193]. These simulations significantly advance our understanding of the underlying mechanisms of membrane remodeling both in biological and artificial systems, and provide means for the controlled design of complex membrane structures [88, 91, 194, 195].

4 Polymerized membrane models

In contrast to fluid membranes, polymerized membranes possess shear elasticity and lack membrane fluidity. An important example of polymerized membranes is a RBC, whose membrane consists of a lipid bilayer with an attached network of spectrin proteins [62]. The spectrin network supplies membrane elasticity that often dominates over additional contributions from the lipid bilayer. Polymerized membranes are represented by solid-like elastic surfaces, which can be simulated using network-based particle models [35, 37, 41, 47, 48, 50, 109, 196, 197] as well as continuum models [14, 38–40, 53, 161, 198–200].

4.1 Bead-spring model of a polymerized membrane

A polymerized membrane (e.g., RBC) can be modeled as a triangular network of springs with N_v vertices, N_e edges, and N_t triangles. The total potential energy of the system is [37, 41, 109, 197]

$$U(\{x_i\}) = U_\mathrm{shear} + U_\mathrm{bend} + U_\mathrm{area} + U_\mathrm{vol}, \tag{15}$$

where $\{x_i\}_{i=1\ldots N_\mathrm{v}}$ is the set of discretization points or membrane vertices. The first term U_shear represents in-plane shear elasticity, the second term U_bend captures membrane bending rigidity, and the last two terms correspond to the constraints of area and volume. The shear elasticity energy is the sum of spring energies within the triangulated spring network given by [41, 109]

$$U_\mathrm{shear} = \sum_{i=1}^{N_e} \frac{k_B T \ell_\mathrm{m}\left(3x_i^2 - 2x_i^3\right)}{4\ell_\mathrm{p}(1-x_i)} + \frac{k_\mathrm{p}}{\ell_i}, \tag{16}$$

where the first part is an attractive worm-like chain potential, while the second term is a repulsive potential. Here, $x_i = \ell_i/\ell_\mathrm{m}$ with the spring length ℓ_i and the maximum spring extension ℓ_m, ℓ_p is the persistence length, k_p is the repulsive coefficient, and k_BT is the energy unit. Linear shear elastic modulus μ_0 of such a network is given by [37, 41, 197]

$$\mu_0 = \frac{\sqrt{3}k_BT}{4p\ell_m x_0}\left(\frac{x_0}{2(1-x_0)^3} - \frac{1}{4(1-x_0)^2} + \frac{1}{4}\right) + \frac{3\sqrt{3}k_p}{4\ell_0^3}, \tag{17}$$

where $x_0 = \ell_0/\ell_m$ with ℓ_0 being the spring length from initial surface triangulation of the membrane.

The bending energy of a polymerized membrane is implemented through the Helfrich curvature energy in Eq. (3) with an example discretization in Eq. (4). The area constraint reads

$$U_\mathrm{area} = \frac{k_\mathrm{a}(A-A_0)^2}{2A_0} + \sum_i^{N_\mathrm{t}} \frac{k_\mathrm{d}\left(A_i - A_i^0\right)^2}{2A_i^0}, \tag{18}$$

consisting of constraint terms for the global and local area. Here, k_a and k_d control the total surface area of the membrane and local area of each triangle, respectively. A is the instantaneous are of the membrane, A_0 is the desired area, A_i is the area of i-th triangle, and A_i^0 is the targeted area of the i-th triangle set from the initial surface triangulation of the membrane. Note that the volume constraint is identical to that for fluid vesicles given in Eq. (6).

In addition to the shear modulus μ_0, Young's Y and area-compression K moduli can be calculated as [37, 41, 197]

$$Y = \frac{2K\mu_0}{K+\mu_0}, \qquad K = 2\mu_0 + k_a + k_d. \tag{19}$$

In practice, macroscopic properties (e.g., μ_0, Y) of the membrane are selected, from which all other parameters of the involved potentials can be deduced. This model has primarily been used for simulations of single RBCs in flow [37, 41, 109, 113–115, 118, 119, 201–203] as well as blood flow with numerous RBCs [110, 116, 204–208].

4.2 Continuum model of a polymerized membrane

In the continuum approach, the membrane surface is represented as a moving Lagrangian mesh, which implements a desired strain energy function. One of the popular strain energy functions for RBCs is given by [209–211]

$$W_\mathrm{m} = \frac{E_\mathrm{s}}{4}\left[\left(\lambda_1^2 + \lambda_2^2 - 2\right)^2 + 2\left(\lambda_1^2 + \lambda_2^2 - \lambda_1^2\lambda_2^2 - 1\right)\right] + \frac{E_\mathrm{a}}{4}\left(\lambda_1^2\lambda_1^2 - 1\right)^2, \tag{20}$$

where λ_1 and λ_2 are the in-plane principle values of strain, E_s is the shear modulus, and E_a is the area-dilation modulus. There also exist other strain functions to describe membrane elasticity [62, 209, 212, 213]. Numerical implementation of membrane elasticity can then be performed through elastic stresses computed as derivatives of the strain energy function W_m [210, 211, 214].

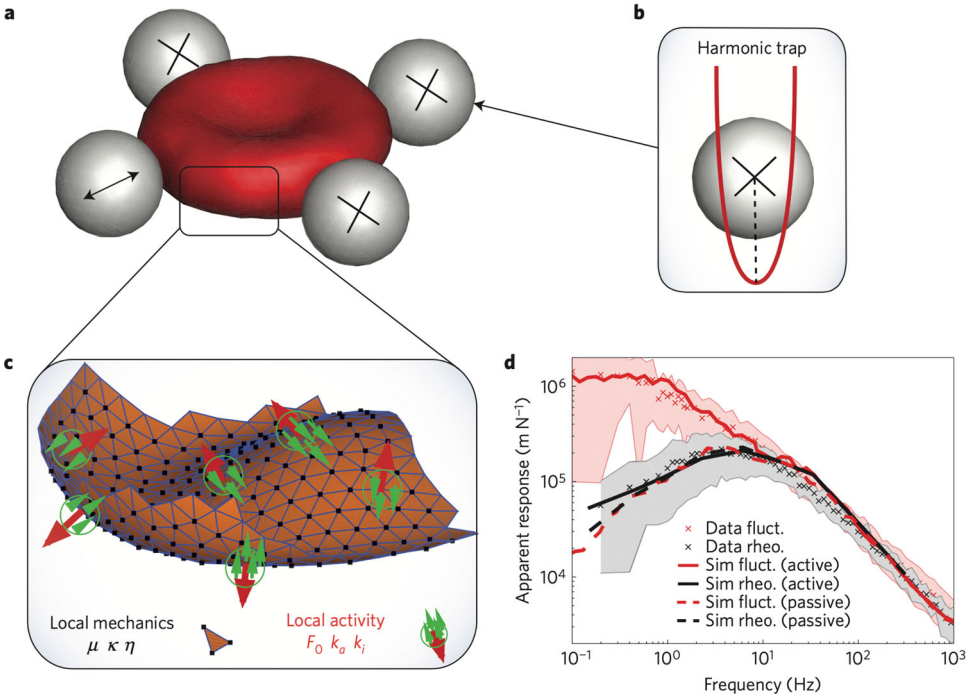

Fig. 6 (**a**) Simulation model mimicking an experimental setup in Ref. [106], where a single RBC with four attached beads is shown. All beads are subject to a harmonic trap illustrated in (**b**). The three beads with the cross-mark are held fixed, while the forth bead can be moved to perform measurements. (**c**) A sketch to illustrate the application of active forces on membrane vertices. Red arrows indicate active forces on selected membrane points, while green arrows represent equal and opposite forces acting on nearby fluid particles. (**d**) Apparent response for both active and passive cases measured from simulations and compared with the experimental data. Reproduced from Ref. [106] with permission from Springer Nature

Incorporation of the bending rigidity in continuum approaches also generally follows the Helfrich's formulation [61, 63, 143] in Eq. (3), for which different discretization strategies can be employed [46, 145–151]. Continuum models of capsules and RBCs have been exploited in various studies, including their dynamics in shear [120, 121, 123, 203, 210, 215–221] and capillary [117, 222, 223] flows, and blood flow in microchannels [112, 224–226] or microvascular networks [227–229].

5 Polymerized membrane applications

5.1 RBC membrane fluctuations

Flickering or fluctuations of a RBC membrane can be observed experimentally [99, 102, 104, 230–232], and are thought to arise from thermal agitation within the surrounding environment. Many previous works [102–104, 232] have employed the measurements of membrane flickering to extract elastic moduli and dissipation of a RBC membrane. Note that the theoretical models [97, 98] used for the interpretation of experimental measurements are based on the assumption of equilibrium thermal fluctuations.

Even though a number of studies [99, 102, 104, 233] have long suggested that RBC flickering may contain active non-equilibrium processes, only recently it was shown that RBC membrane fluctuations indeed contain active contributions [106]. This study consists of optical tweezers experiments, an analytical model, and simulations mimicking the experimental setup [106]. The setup involved the attachment of four beads to a RBC, as illustrated in the Fig. 6a, where the three trapped beads were used to hold the cell, while the fourth probe bead has been employed for measurements. In particular, the probe bead was subjected to a sinusoidally varying force, to measure the response function shown in Fig. 6d. Another measurement is the power spectral density which is derived from monitored fluctuations of the probe bead. In equilibrium, these two measurements are related through the fluctuation–dissipation theorem, which becomes invalid out of equilibrium. This is illustrated in Fig. 6d where a discrepancy in the apparent response is obtained for these two measurements at low frequencies, confirming the presence of non-equilibrium processes. A bead-spring network model [see Sect. 4.1 and Fig. 6a] has been used to quantify elastic properties of the RBC membrane and the strength of active stresses. In this model, active

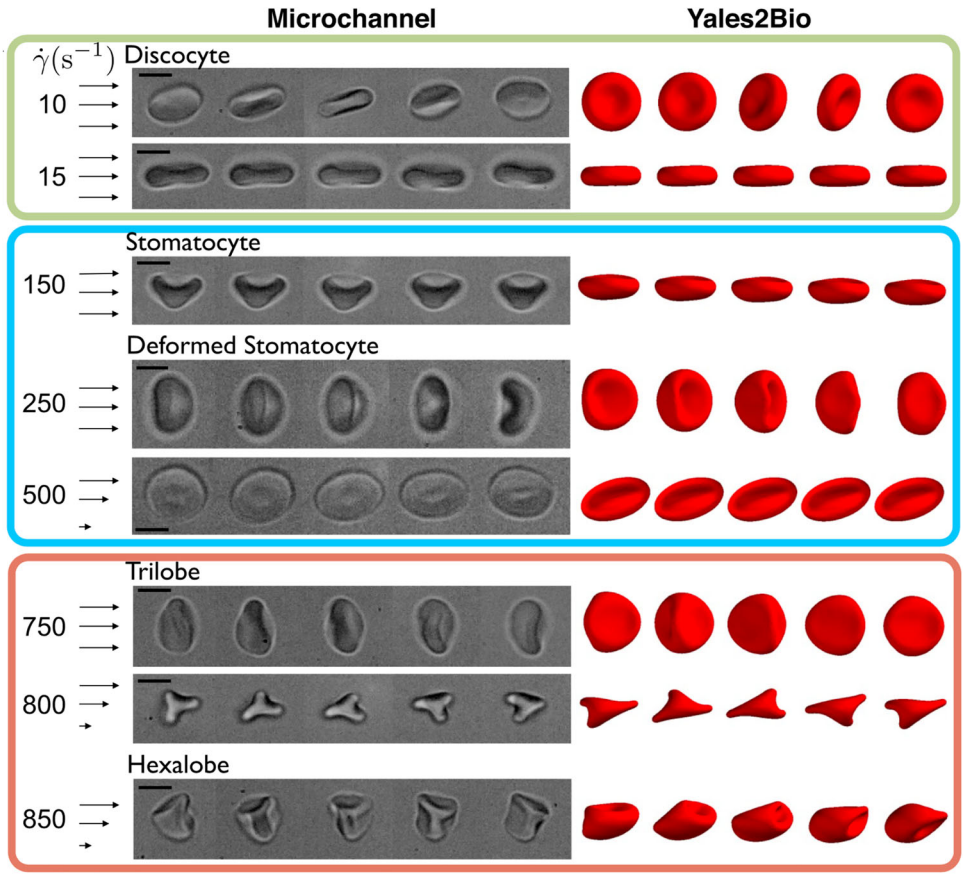

Fig. 7 RBC snapshots in shear flow (left) accompanied by similar images from continuum (Yales2Bio [199]) simulations (right). The snapshots are shown for various shear rates, ranging from 10 s^{-1} to 850 s^{-1}. At small shear rates, tumbling and rolling of RBCs is observed, whereas intermediate shear rates result in rolling or tumbling stomatocytic shapes. At high shear rates, polylobe shapes are observed, including trilobes and hexalobes. Re-used with permission from Ref. [116]

forces were added to randomly selected membrane vertices [see Fig. 6c], which acted in the normal direction to the membrane. For momentum conservation, equal and opposite forces were applied to nearby fluid particles. The simulation data in Fig. 6d aligns well with the experimental measurements, and further supports the presence of non-equilibrium processes within a RBC membrane. Note that the exact source of active contributions to RBC flickering remains unknown, with several suggestions such as active remodeling of the spectrin network, the activity of membrane channels, and curvature-inducing intra-membrane components [234–237].

5.2 RBC deformation in flow

To better understand RBC behavior in blood flow, it is essential to study RBC dynamics under different flow conditions which span the wide range of microcirculatory characteristics. RBC deformation in response to fluid stresses is important not only for the characterization of single cell behavior under dilute conditions [37, 41, 114, 120, 123, 203, 216, 217, 220, 221], but also for understanding changes in blood viscosity, and blood-flow resistance in the microvasculature [112, 116, 205, 206, 224–226]. Figure 7 compares various RBC morphologies at different shear rates in shear flow between experiments and simulations [116]. With increasing shear rate, RBCs transit from tumbling and rolling biconcave discocytes, to rolling stomatocytes, and multilobar morphologies at shear rates beyond approximately 1000 s^{-1}. These dynamic changes in RBC shapes can be connected to the shear-thinning characteristics of blood viscosity, which decreases with increasing shear rate. Experimental observations have also been supported by continuum and particle-based models of RBCs with quantitatively consistent predictions [116].

In large enough vessels, the behavior of RBCs is similar to that in shear flow, as the local shear rate on the scale of RBC size can be considered constant. In capillaries, whose diameter is comparable with the RBC size, several other shapes appear, including parachutes and slippers [108, 109, 111, 115, 117–119, 201, 202]. Parachutes are nearly symmetric stomatocyte-like shapes that develop due to the curvature of the flow profile [109, 115, 118]. Slippers are non-symmetric shapes, located off-center of the capillary due to the instability of parachute shapes under certain conditions [115, 118, 119]. For channels with a rectangular cross-section, parachute shapes loose axisymmetry and resemble crescent shapes [117]. Note that the transitions between different shapes in microchannels depend on various parameters such as channel size, flow rate, RBC membrane elasticity, and the viscosity contrast between cell cytosol and suspending plasma [115, 117–119].

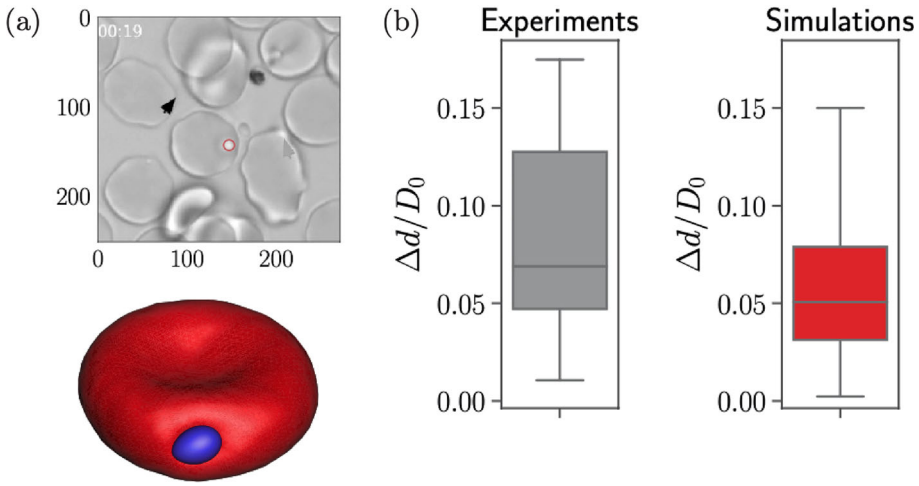

Fig. 8 (**a**) Snapshots showing a merozoite interacting with a RBC from experimental observations (top) and simulations (bottom). (**b**) Parasite displacements on the RBC membrane measured from experimental data and simulations. Re-used with permission from Ref. [131]

5.3 Adhesion of malaria parasites to erythrocytes

Merozoite, a malaria parasite during the blood stage of infection, invades RBCs to multiply inside the cells and facilitate further disease progression [238]. After merozoite adhesion to a RBC membrane, the invasion process can only start when a direct contact between the parasite's apex (i.e., a small region at the merozoite surface) and the membrane is established [125, 239]. Since initial adhesion of the parasite likely has an arbitrary orientation, it is hypothesized that adhered parasites can re-orient themselves to form the apex-membrane contact. Recent experiments report that RBC invasion starts approximately $10-20$ seconds after the initial merozoite attachment [128, 240], during which RBC membrane often shows strong deformations and the parasite actively moves at the membrane.

Recent simulation study [131] has considered the re-orientation (or alignment) process, and the role of membrane deformations, see Fig. 8a. The adhesion of a rigid parasite to RBC membrane was modeled through discrete bindings, whose dynamics is governed by kinetic association/dissociation rates. Weak adhesion may not be sufficient to keep contact between the merozoite and the membrane, while strong adhesion leads to an arrest of the adhered parasite without visible motion. For intermediate adhesion strengths, the adhered parasite exhibits kinetic-rate dependent motion, whose characteristics are calibrated by the experimental measurements [128, 240] and shown in Fig. 8b. After the calibration of adhered parasite dynamics, the alignment time of the merozoite agreed well with the mean alignment time measured experimentally. The alignment process is an intricate balance between membrane deformation and parasite dynamics, which was quantified by simulations [130–132]. Interestingly, simulations suggest that no additional active processes are required for the efficient parasite alignment. Furthermore, simulations have shown that the alignment time drastically increases for cells with an increased membrane stiffness which is directly relevant to the fact that malaria progression is poor for some blood disorders such as sickle-cell anemia [241]. An accompanying study has looked into the effect of different parasite shapes, and showed that the natural egg-like shape of a merozoite results in favorable alignment timescales in comparison to other possible shapes [132].

6 Conclusions

In this review, we have focused on the models which represent membranes as 2D surfaces and allow membrane modeling at the cellular scale. Two distinct classes of models have been considered, including fluid membrane and polymerized membrane models. Numerical implementation of these models can proceed through a variety of approaches, including particle-based simulation techniques and continuum modeling approaches. These models are already powerful enough to capture the behavior of complex membrane systems, which has been illustrated through a number of recent simulation studies.

Despite many successful developments and applications of the 2D surface models of membranes, these approaches fully sacrifice atomistic details. As a result, these models cannot directly capture chemical specificity of different molecular components of the membrane. Some of the molecular effects can be incorporated phenomenologically into these models, as it is done for the modeling of curvature-inducing proteins [88, 91, 92, 187]. To accurately simulate real membrane systems, a direct mapping between atomistic and thin-surface membrane models would be desirable, which is the topic of several recent studies [196, 242–244].

As we move toward the modeling of realistic biological systems, another important aspect of membrane models is the incorporation of active non-equilibrium processes. Several models have considered the presence of active stresses within the membrane, which are supposed to mimic certain non-equilibrium processes [106, 245–247]. Despite the fact that these active membrane models are very useful for the elucidation of relevant physical mechanisms, they do not provide a direct connection to the underlying non-equilibrium processes. This motivates the development of more complex models, where the existing membrane approaches are combined with the explicit modeling of other relevant components. Examples include vesicles with active particles [71, 73–79] discussed in Sect. 3.1, a double-layer model of RBCs with the explicit representation of both lipid bilayer and spectrin cytoskeleton [196, 248, 249], and membranes with the explicit modeling of internal cytoskeletal structures [250]. Furthermore, several membrane models implement reaction-diffusion equations to represent the spatio-temporal distribution of molecular components, which may control local active stresses or curvature [90, 247, 251]

In conclusion, mesoscopic 2D-surface models of membranes are very versatile and suitable for modeling cellular-scale phenomena. They play a crucial role in the characterization of many biological and artificial membrane systems. However, to achieve the necessary computational efficiency for studying cellular processes, these models sacrifice the ability to resolve nanoscale phenomena such as lipid heterogeneity and phase separation. Their continuous development and integration with other models highlight their importance, and bring us closer to realistic and comprehensive models of biological cells and cell-mimicking artificial systems.

Data availability statement No data are associated with this manuscript.

References

1. P. Bassereau, P. Sens, editors. *Physics of Biological Membranes*. Springer, Cham, first edition, (2018)
2. J.T. Groves, J. Kuriyan, Molecular mechanisms in signal transduction at the membrane. Nat. Struct. Mol. Biol. **17**, 659–665 (2010)
3. M. Doktorova, J.L. Symons, I. Levental, Structural and functional consequences of reversible lipid asymmetry in living membranes. Nat. Chem. Biol. **16**, 1321–1330 (2020)
4. H.T. McMahon, J.L. Gallop, Membrane curvature and mechanisms of dynamic cell membrane remodelling. Nature **438**, 590–596 (2005)
5. J.G. Carlton, H. Jones, U.S. Eggert, Membrane and organelle dynamics during cell division. Nat. Rev. Mol. Cell Biol. **21**, 151–166 (2020)
6. A. Diz-Muñoz, D.A. Fletcher, O.D. Weiner, Use the force: membrane tension as an organizer of cell shape and motility. Trends Cell Biol. **23**, 47–53 (2013)
7. K.M. Yamada, M. Sixt, Mechanisms of 3D cell migration. Nat. Rev. Mol. Cell Biol. **20**, 738–752 (2019)
8. G. van Meer, D.R. Voelker, G.W. Feigenson, Membrane lipids: where they are and how they behave. Nat. Rev. Mol. Cell Biol. **9**, 112–124 (2008)
9. R. Phillips, J. Kondev, J. Theriot, H. Garcia, *Physical Biology of the Cell* (New York, second edition, Garland Science, 2012)
10. B.M. Discher, Y.-Y. Won, D.S. Ege, J.C.-M. Lee, F.S. Bates, D.E. Discher, D.A. Hammer, Polymersomes: tough vesicles made from diblock copolymers. Science **284**, 1143–1146 (1999)
11. V. Percec, D.A. Wilson, P. Leowanawat, C.J. Wilson, A.D. Hughes, M.S. Kaucher, D.A. Hammer, D.H. Levine, A.J. Kim, F.S. Bates, K.P. Davis, T.P. Lodge, M.L. Klein, R.H. DeVane, E. Aqad, B.M. Rosen, A.O. Argintaru, M.J. Sienkowska, K. Rissanen, S. Nummelin, J. Ropponen, Self-assembly of Janus dendrimers into uniform dendrimersomes and other complex architectures. Science **328**, 1009–1014 (2010)
12. A. M. Wagner, J. Quandt, D. Söder, M. Garay-Sarmiento, A. Joseph, V. S. Petrovskii, L. Witzdam, T. Hammoor, P. Steitz, Haraszti T., Potemkin I. I., Kostina N. Y., A. Herrman, C. Rodriguez-Emmenegger, Ionic combisomes: a new class of biomimetic vesicles to fuse with life. *Adv. Sci.*, 9:2200617, (2022)
13. D.A. Fedosov, H. Noguchi, G. Gompper, Multiscale modeling of blood flow: from single cells to blood rheology. Biomech. Model. Mechanobiol. **13**, 239–258 (2014)
14. J.B. Freund, Numerical simulation of flowing blood cells. Annu. Rev. Fluid Mech. **46**, 67–95 (2014)
15. S.J. Marrink, V. Corradi, P.C.T. Souza, H.I. Ingólfsson, D.P. Tieleman, M.S.P. Sansom, Computational modeling of realistic cell membranes. Chem. Rev. **119**, 6184–6226 (2019)
16. T. Auth, D. A. Fedosov, G. Gompper. Simulating membranes, vesicles, cells. In R. Dimova and C. Marques, editors, *The giant vesicle book*. CRC Press, 2019
17. G. Kumar, S.C. Duggisetty, A. Srivastava, A review of mechanics-based mesoscopic membrane remodeling methods: capturing both the physics and the chemical diversity. J. Mem. Biol. **255**, 757–777 (2022)
18. G. Gompper, D.A. Fedosov, Modeling microcirculatory blood flow: current state and future perspectives. WIREs Syst. Biol. Med. **8**, 157–168 (2016)
19. A.L. Duncan, W. Pezeshkian, Mesoscale simulations: an indispensable approach to understand biomembranes. Biophys. J. **122**, 1883–1889 (2023)
20. H. Noguchi, Membrane simulation models from nanometer to micrometer scale. J. Phys. Soc. Jpn. **78**, 041007 (2009)

21. D.P. Tieleman, S.J. Marrink, H.J.C. Berendsen, A computer perspective of membranes: molecular dynamics studies of lipid bilayer systems. Biochim. Biophys. Acta **1331**, 235–270 (1997)
22. E.H. Lee, J. Hsin, M. Sotomayor, G. Comellas, K. Schulten, Discovery through the computational microscope. Structure **17**, 1295–1306 (2009)
23. A.A. Skjevik, B.D. Madej, C.J. Dickson, C. Lin, K. Teigen, R.C. Walker, I.R. Gould, Simulation of lipid bilayer self-assembly using all-atom lipid force fields. Phys. Chem. Chem. Phys. **18**, 10573–10584 (2016)
24. A.P. Lyubartsev, A.L. Rabinovich, Recent development in computer simulations of lipid bilayers. Soft Matter **7**, 25–39 (2011)
25. C.J. Dickson, B.D. Madej, A.A. Skjevik, R.M. Betz, K. Teigen, I.R. Gould, R.C. Walker, Lipid14: the amber lipid force field. J. Chem. Theory Comput. **10**, 865–879 (2014)
26. P.M. Kasson, E. Lindahl, V.S. Pande, Atomic-resolution simulations predict a transition state for vesicle fusion defined by contact of a few lipid tails. PLoS Comput. Biol. **6**, e1000829 (2010)
27. R. Goetz, G. Gompper, R. Lipowsky, Mobility and elasticity of self-assembled membranes. Phys. Rev. Lett. **82**, 221–224 (1999)
28. J.C. Shillcock, R. Lipowsky, Equilibrium structure and lateral stress distribution of amphiphilic bilayers from dissipative particle dynamics simulations. J. Chem. Phys. **117**, 5048–5061 (2002)
29. S.J. Marrink, A.E. Mark, Molecular dynamics simulation of the formation, structure, dynamics of small phospholipid vesicles. J. Am. Chem. Soc. **125**, 15233–15242 (2003)
30. M. Laradji, P.B.S. Kumar, Dynamics of domain growth in self-assembled fluid vesicles. Phys. Rev. Lett. **93**, 198105 (2004)
31. I.R. Cooke, K. Kremer, M. Deserno, Tunable generic model for fluid bilayer membranes. Phys. Rev. E **72**, 011506 (2005)
32. M. Deserno, Mesoscopic membrane physics: concepts, simulations, selected applications. Macromol. Rapid Commun. **30**, 752–771 (2009)
33. W.K. den Otter, W.J. Briels, The bending rigidity of an amphiphilic bilayer from equilibrium and nonequilibrium molecular dynamics. J. Chem. Phys. **118**, 4712–4720 (2003)
34. J.M. Drouffe, A.C. Maggs, S. Leibler, Computer simulations of self-assembled membranes. Science **254**, 1353–1356 (1991)
35. G. Gompper, D. M. Kroll, Network models of fluid, hexatic and polymerized membranes. *J. Phys.: Condens. Matter*, 9:8795–8834, (1997)
36. H. Noguchi, G. Gompper, Meshless membrane model based on the moving least-squares method. Phys. Rev. E **73**, 021903 (2006)
37. I.V. Pivkin, G.E. Karniadakis, Accurate coarse-grained modeling of red blood cells. Phys. Rev. Lett. **101**, 118105 (2008)
38. S.K. Doddi, P. Bagchi, Three-dimensional computational modeling of multiple deformable cells flowing in microvessels. Phys. Rev. E **79**, 046318 (2009)
39. H. Zhao, A.H.G. Isfahani, L.N. Olson, J.B. Freund, A spectral boundary integral method for flowing blood cells. J. Comput. Phys. **229**, 3726–3744 (2010)
40. R.M. MacMeccan, J.R. Clausen, G.P. Neitzel, C.K. Aidun, Simulating deformable particle suspensions using a coupled lattice-Boltzmann and finite-element method. J. Fluid Mech. **618**, 13–39 (2009)
41. D.A. Fedosov, B. Caswell, G.E. Karniadakis, A multiscale red blood cell model with accurate mechanics, rheology, dynamics. Biophys. J. **98**, 2215–2225 (2010)
42. G. Brannigan, F.L.H. Brown, Solvent-free simulations of fluid membrane bilayers. J. Chem. Phys. **120**, 1059–1071 (2004)
43. P. Ballone, M.G. Del Pópolo, Simple models of complex aggregation: vesicle formation by soft repulsive spheres with dipolelike interactions. Phys. Rev. E **73**, 031404 (2006)
44. T. Kohyama, Simulations of flexible membranes using a coarse-grained particle-based model with spontaneous curvature variables. Phys. A **388**, 3334–3344 (2009)
45. H. Yuan, C. Huang, J. Li, G. Lykotrafitis, S. Zhang, One-particle-thick, solvent-free, coarse-grained model for biological and biomimetic fluid membranes. Phys. Rev. E **82**, 011905 (2010)
46. G. Gompper, D. M. Kroll, Triangulated-surface models of fluctuating membranes. In D. R. Nelson, T. Piran, S. Weinberg, editors, *Statistical mechanics of membranes and surfaces*, pages 359–426. World Scientific, Singapore, 2nd edition, (2004)
47. S.K. Boey, D.H. Boal, D.E. Discher, Simulations of the erythrocyte cytoskeleton at large deformation. I. Microscopic models. Biophys. J. **75**, 1573–1583 (1998)
48. J. Li, G. Lykotrafitis, M. Dao, S. Suresh, Cytoskeletal dynamics of human erythrocyte. Proc. Natl. Acad. Sci. USA **104**, 4937–4942 (2007)
49. E. Atilgan, S.X. Sun, Shape transitions in lipid membranes and protein mediated vesicle fusion and fission. J. Chem. Phys. **126**, 095102 (2007)
50. J. Li, M. Dao, C.T. Lim, S. Suresh, Spectrin-level modeling of the cytoskeleton and optical tweezers stretching of the erythrocyte. Biophys. J. **88**, 3707–3719 (2005)
51. T. Biben, K. Kassner, C. Misbah, Phase-field approach to three-dimensional vesicle dynamics. Phys. Rev. E **72**, 041921 (2005)

52. F. Feng, W.S. Klug, Finite element modeling of lipid bilayer membranes. J. Comput. Phys. **220**, 394–408 (2006)
53. Z. Peng, R.J. Asaro, Q. Zhu, Multiscale modelling of erythrocytes in Stokes flow. J. Fluid Mech. **686**, 299–337 (2011)
54. T. Krüger, F. Varnik, D. Raabe, Efficient and accurate simulations of deformable particles immersed in a fluid using a combined immersed boundary lattice Boltzmann finite element method. Comput. Math. Appl. **61**, 3485–3505 (2011)
55. T. Omori, Y. Imai, K. Kikuchi, T. Ishikawa, T. Yamaguchi, Hemodynamics in the microcirculation and in microfluidics. Ann. Biomed. Eng. **43**, 238–257 (2015)
56. D.A. Fedosov, M. Dao, G.E. Karniadakis, S. Suresh, Computational biorheology of human blood flow in health and disease. Ann. Biomed. Eng. **42**, 368–387 (2014)
57. X. Li, P.M. Vlahovska, G.E. Karniadakis, Continuum- and particle-based modeling of shapes and dynamics of red blood cells in health and disease. Soft Matter **9**, 28–37 (2013)
58. M. Ju, S.S. Ye, B. Namgung, S. Cho, H.T. Low, H.L. Leo, S. Kim, A review of numerical methods for red blood cell flow simulation. Computer Meth. Biomech. Biomed. Eng. **18**, 130–140 (2015)
59. F.J. Alenghat, D.E. Golan, Membrane protein dynamics and functional implications in mammalian cells. Curr. Top. Membr. **72**, 89–120 (2013)
60. A.-S. Smith, K. Sengupta, S. Goennenwein, U. Seifert, E. Sackmann, Force-induced growth of adhesion domains is controlled by receptor mobility. Proc. Natl. Acad. Sci. USA **105**, 6906–6911 (2008)
61. R. Lipowsky, The conformation of membranes. Nature **349**, 475–481 (1991)
62. E.A. Evans, R. Skalak, *Mechanics and thermodynamics of biomembranes* (CRC Press Inc, Boca Raton, 1980)
63. W. Helfrich, Elastic properties of lipid bilayers: theory and possible experiments. Z. Naturforsch. **28**, 693–703 (1973)
64. U.S. Schwarz, M.L. Gardel, United we stand - integrating the actin cytoskeleton and cell-matrix adhesions in cellular mechanotransduction. J. Cell Sci. **125**, 3051–3060 (2012)
65. J. Plastino, L. Blanchoin, Dynamic stability of the actin ecosystem. J. Cell Sci. **132**, 219832 (2019)
66. K.S. Chang, W.L. Olbricht, Experimental studies of the deformation and breakup of a synthetic capsule in steady and unsteady simple shear flow. J. Fluid Mech. **250**, 609–633 (1993)
67. P. Erni, P. Fisher, Windhab E. Deformation of single emulsion drops covered with a viscoelastic adsorbed protein layer in simple shear flow. *Appl. Phys. Lett.*, 87:244104, 2005
68. D. Barthés-Biesel, Modeling the motion of capsules in flow. Curr. Opin. Colloid Interface Sci. **16**, 3–12 (2011)
69. D. Barthés-Biesel, Mechanics of encapsulated droplets. Progr. Colloid. Polym. Sci. **111**, 58–64 (1998)
70. D.R. Nelson, T. Piran, S. Weinberg, *Statistical mechanics of membranes and surfaces*, 2nd edn. (World Scientific, Singapore, 2004)
71. H.R. Vutukuri, M. Hoore, C. Abaurrea-Velasco, L. van Buren, A. Dutto, T. Auth, D.A. Fedosov, G. Gompper, J. Vermant, Active particles induce large shape deformations in giant lipid vesicles. Nature **586**, 52–56 (2020)
72. S.C. Takatori, A. Sahu, Active contact forces drive nonequilibrium fluctuations in membrane vesicles. Phys. Rev. Lett. **124**, 158102 (2020)
73. M. Paoluzzi, R. Di Leonardo, M.C. Marchetti, L. Angelani, Shape and displacement fluctuations in soft vesicles filled by active particles. Sci. Rep. **6**, 34146 (2016)
74. J. Chen, Y. Hua, Y. Jiang, X. Zhou, L. Zhang, Rotational diffusion of soft vesicles filled by chiral active particles. Sci. Rep. **7**, 15006 (2017)
75. Y. Li, P.R. ten Wolde, Shape transformations of vesicles induced by swim pressure. Phys. Rev. Lett. **123**, 148003 (2019)
76. C. Wang, Y. Guo, W. Tian, K. Chen, Shape transformation and manipulation of a vesicle by active particles. J. Chem. Phys. **150**, 044907 (2019)
77. M.S.E. Peterson, A. Baskaran, M.F. Hagan, Vesicle shape transformations driven by confined active filaments. Nat. Comm. **12**, 7247 (2021)
78. P. Iyer, G. Gompper, D.A. Fedosov, Non-equilibrium shapes and dynamics of active vesicles. Soft Matter **18**, 6868–6881 (2022)
79. P. Iyer, G. Gompper, D.A. Fedosov, Dynamic shapes of floppy vesicles enclosing active Brownian particles with membrane adhesion. Soft Matter **19**, 3436–3449 (2023)
80. L. Le Nagard, A.T. Brown, A. Dawson, V.A. Martinez, W.C.K. Poon, M. Staykova, Encapsulated bacteria deform lipid vesicles into flagellated swimmers. Proc. Natl. Acad. Sci. USA **119**, e2206096119 (2022)
81. T. Wollert, C. Wunder, J. Lippincott-Schwartz, J.H. Hurley, Membrane scission by the ESCRT-III complex. Nature **458**, 172–177 (2009)
82. L. Harker-Kirschneck, B. Baum, A. Šarić, Changes in ESCRT-III filament geometry drive membrane remodelling and fission in silico. BMC Biol. **17**, 82 (2019)
83. M. Lenz, D.J.G. Crow, J.-F. Joanny, Membrane buckling induced by curved filaments. Phys. Rev. Lett. **103**, 038101 (2009)
84. G. Fabrikant, S. Lata, J.D. Riches, J.A.G. Briggs, W. Weissenhorn, M.M. Kozlov, Computational model of membrane fission catalyzed by ESCRT-III. PLoS Comput. Biol. **5**, e1000575 (2009)
85. J. Agudo-Canalejo, R. Lipowsky, Domes and cones: adhesion-induced fission of membranes by ESCRT proteins. PLoS Comput. Biol. **14**, e1006422 (2018)
86. O. Daumke, A. Roux, V. Haucke, BAR domain scaffolds in dynamin-mediated membrane fission. Cell **156**, 882–892 (2014)

87. W. Römer, L. Berland, V. Chambon, K. Gaus, B. Windschiegl, D. Tenza, M.R.E. Aly, V. Fraisier, J.-C. Florent, D. Perrais, C. Lamaze, G. Raposo, C. Steinem, P. Sens, P. Bassereau, L. Johannes, Shiga toxin induces tubular membrane invaginations for its uptake into cells. Nature **450**, 670–675 (2007)
88. N. Ramakrishnan, P.B.S. Kumar, J.H. Ipsen, Membrane-mediated aggregation of curvature-inducing nematogens and membrane tubulation. Biophys. J. **104**, 1018–1028 (2013)
89. P. Rangamani, K.K. Mandadap, G. Oster, Protein-induced membrane curvature alters local membrane tension. Biophys. J. **107**, 751–762 (2014)
90. N.S. Gov, Guided by curvature: shaping cells by coupling curved membrane proteins and cytoskeletal forces. Phil. Trans. R. Soc. B **373**, 20170115 (2018)
91. W. Pezeshkian, J.H. Ipsen, Fluctuations and conformational stability of a membrane patch with curvature inducing inclusions. Soft Matter **15**, 9974–9981 (2019)
92. H. Noguchi, C. Tozzi, M. Arroyo, Binding of anisotropic curvature-inducing proteins onto membrane tubes. Soft Matter **18**, 3384–3394 (2022)
93. H. Noguchi, Vesicle budding induced by binding of curvature-inducing proteins. Phys. Rev. E **104**, 014410 (2021)
94. J. Steinkühler, R.L. Knorr, Z. Zhao, T. Bhatia, S.M. Bartelt, S. Wegner, R. Dimova, R. Lipowsky, Controlled division of cell-sized vesicles by low densities of membrane-bound proteins. Nat. Comm. **11**, 905 (2020)
95. T. Bhatia, S. Christ, J. Steinkühler, R. Dimova, R. Lipowsky, Simple sugars shape giant vesicles into multispheres with many membrane necks. Soft Matter **16**, 1246–1258 (2020)
96. R. Lipowsky, Multispherical shapes of vesicles highlight the curvature elasticity of biomembranes. Adv. Colloid Interface Sci. **301**, 102613 (2022)
97. F. Brochard, J.F. Lennon, Frequency spectrum of the flicker phenomenon in erythrocytes. J. Phys. **36**, 1035–1047 (1975)
98. H. Strey, M. Peterson, E. Sackmann, Measurement of erythrocyte membrane elasticity by flicker eigenmode decomposition. Biophys. J. **69**, 478–488 (1995)
99. S. Tuvia, A. Almagor, A. Bitler, S. Levin, R. Korenstein, S. Yedgar, Cell membrane fluctuations are regulated by medium macroviscosity: evidence for a metabolic driving force. Proc. Natl. Acad. Sci. USA **94**, 5045–5049 (1997)
100. N. Gov, S.A. Safran, Red blood cell shape and fluctuations: cytoskeleton confinement and ATP activity. J. Biol. Phys. **31**, 453–464 (2005)
101. G. Marcelli, K.H. Parker, C.P. Winlove, Thermal fluctuations of red blood cell membrane via a constant-area particle-dynamics model. Biophys. J. **89**, 2473–2480 (2005)
102. T. Betz, M. Lenz, J.-F. Joanny, C. Sykes, ATP-dependent mechanics of red blood cells. Proc. Natl. Acad. Sci. USA **106**, 15320–15325 (2009)
103. J.P. Hale, G. Marcelli, K.H. Parker, C.P. Winlove, P.G. Petrov, Red blood cell thermal fluctuations: comparison between experiment and molecular dynamics simulations. Soft Matter **5**, 3603–3606 (2009)
104. Y.-K. Park, C.A. Best, T. Auth, N.S. Gov, S.A. Safran, G. Popescu, S. Suresh, M.S. Feld, Metabolic remodeling of the human red blood cell membrane. Proc. Natl. Acad. Sci. USA **107**, 1289–1294 (2010)
105. E. Ben-Isaac, Y.-K. Park, G. Popescu, F.L.H. Brown, N.S. Gov, Y. Shokef, Effective temperature of red-blood-cell membrane fluctuations. Phys. Rev. Lett. **106**, 238103 (2011)
106. H. Turlier, D.A. Fedosov, B.A. Audoly, T. Auth, N.S. Gov, C. Sykes, J.-F. Joanny, G. Gompper, T. Betz, Equilibrium physics breakdown reveals the active nature of red blood cell membrane fluctuations. Nat. Phys. **12**, 513–519 (2016)
107. A.A. Evans, B. Bhaduri, G. Popescu, A.J. Levine, Geometric localization of thermal fluctuations in red blood cells. Proc. Natl. Acad. Sci. USA **114**, 2865–2870 (2017)
108. M. Abkarian, M. Faivre, R. Horton, K. Smistrup, C.A. Best-Popescu, H.A. Stone, Cellular-scale hydrodynamics. Biomed. Mater. **3**, 034011 (2008)
109. H. Noguchi, G. Gompper, Shape transitions of fluid vesicles and red blood cells in capillary flows. Proc. Natl. Acad. Sci. USA **102**, 14159–14164 (2005)
110. J.L. McWhirter, H. Noguchi, G. Gompper, Flow-induced clustering and alignment of vesicles and red blood cells in microcapillaries. Proc. Natl. Acad. Sci. USA **106**, 6039–6043 (2009)
111. G. Tomaiuolo, M. Simeone, V. Martinelli, B. Rotoli, S. Guido, Red blood cell deformation in microconfined flow. Soft Matter **5**, 3736–3740 (2009)
112. J.B. Freund, M.M. Orescanin, Cellular flow in a small blood vessel. J. Fluid Mech. **671**, 466–490 (2011)
113. H. Noguchi, Dynamic modes of red blood cells in oscillatory shear flow. Phys. Rev. E **81**, 061920 (2010)
114. H. Noguchi, Swinging and synchronized rotations of red blood cells in simple shear flow. Phys. Rev. E **80**, 021902 (2009)
115. D.A. Fedosov, M. Peltomäki, G. Gompper, Deformation and dynamics of red blood cells in flow through cylindrical microchannels. Soft Matter **10**, 4258–4267 (2014)
116. L. Lanotte, J. Mauer, S. Mendez, D.A. Fedosov, J.-M. Fromental, V. Claveria, F. Nicoud, G. Gompper, M. Abkarian, Red cells' dynamic morphologies govern blood shear thinning under microcirculatory flow conditions. Proc. Natl. Acad. Sci. USA **113**, 13289–13294 (2016)
117. A. Guckenberger, A. Kihm, T. John, C. Wagner, S. Gekle, Numerical-experimental observation of shape bistability of red blood cells flowing in a microchannel. Soft Matter **14**, 2032–2043 (2018)
118. F. Reichel, J. Mauer, A.A. Nawaz, G. Gompper, J. Guck, D.A. Fedosov, High-throughput microfluidic characterization of erythrocyte shapes and mechanical variability. Biophys. J. **117**, 14–24 (2019)

119. A.K. Dasanna, J. Mauer, G. Gompper, D.A. Fedosov, Importance of viscosity contrast for the motion of erythrocytes in microcapillaries. Front. Phys. **9**, 666913 (2021)
120. K. Sinha, M.D. Graham, Dynamics of a single red blood cell in simple shear flow. Phys. Rev. E **92**, 042710 (2015)
121. D. Cordasco, P. Bagchi, Orbital drift of capsules and red blood cells in shear flow. Phys. Fluids **25**, 091902 (2013)
122. D. Cordasco, A. Yazdani, P. Bagchi, Comparison of erythrocyte dynamics in shear flow under different stress-free configurations. Phys. Fluids **26**, 041902 (2014)
123. A.Z.K. Yazdani, P. Bagchi, Phase diagram and breathing dynamics of a single red blood cell and a biconcave capsule in dilute shear flow. Phys. Rev. E **84**, 026314 (2011)
124. A.Z.K. Yazdani, R.M. Kalluri, P. Bagchi, Tank-treading and tumbling frequencies of capsules and red blood cells. Phys. Rev. E **83**, 046305 (2011)
125. A.F. Cowman, B.S. Crabb, Invasion of red blood cells by malaria parasites. Cell **124**, 755–766 (2006)
126. S. Dasgupta, T. Auth, N. Gov, T.J. Satchwell, E. Hanssen, E.S. Zuccala, D.T. Riglar, A.M. Toye, T. Betz, J. Baum, G. Gompper, Membrane-wrapping contributions to malaria parasite invasion of the human erythrocyte. Biophys. J. **107**, 43–54 (2014)
127. A.J. Crick, M. Theron, T. Tiffert, V.L. Lew, P. Cicuta, J.C. Rayner, Quantitation of malaria parasite-erythrocyte cell-cell interactions using optical tweezers. Biophys. J. **107**, 846–853 (2014)
128. G.E. Weiss, P.R. Gilson, T. Taechalertpaisarn, W.-H. Tham, N.W.M. de Jong, K.L. Harvey, F.J.I. Fowkes, P.N. Barlow, J.C. Rayner, G.J. Wright, A.F. Cowman, B.S. Crabb, Revealing the sequence and resulting cellular morphology of receptor-ligand interactions during Plasmodium falciparum invasion of erythrocytes. PLoS Pathog. **11**, e1004670 (2015)
129. V. Introini, A. Carciati, G. Tomaiuolo, P. Cicuta, S. Guido, Endothelial glycocalyx regulates cytoadherence in Plasmodium falciparum malaria. J. R. Soc. Interface **15**, 20180773 (2018)
130. S. Hillringhaus, A.K. Dasanna, G. Gompper, D.A. Fedosov, Importance of erythrocyte deformability for the alignment of malaria parasite upon invasion. Biophys. J. **117**, 1202–1214 (2019)
131. S. Hillringhaus, A.K. Dasanna, G. Gompper, D.A. Fedosov, Stochastic bond dynamics facilitates alignment of malaria parasite at erythrocyte membrane upon invasion. eLife **9**, e56500 (2020)
132. A.K. Dasanna, S. Hillringhaus, G. Gompper, D.A. Fedosov, Effect of malaria parasite shape on its alignment at erythrocyte membrane. eLife **10**, e68818 (2021)
133. D.M. Kroll, G. Gompper, The conformation of fluid membranes: Monte Carlo simulations. Science **255**, 968–971 (1992)
134. D.H. Boal, M. Rao, Topology changes in fluid membranes. Phys. Rev. A **46**, 3037–3045 (1992)
135. S.-J. Zhao, J.T. Kindt, Monte Carlo calculations of the free-energy landscape of vesicle formation and growth. Europhys. Lett. **69**, 839–845 (2005)
136. J.-S. Ho, A. Baumgärtner, Simulations of fluid self-avoiding membranes. Europhys. Lett. **12**, 295–300 (1990)
137. H. Zhao, E.S.G. Shaqfeh, The dynamics of a vesicle in simple shear flow. J. Fluid Mech. **674**, 578–604 (2011)
138. S.K. Veerapaneni, A. Rahimian, G. Biros, D. Zorin, A fast algorithm for simulating vesicle flows in three dimensions. J. Comput. Phys. **230**, 5610–5634 (2011)
139. Q. Du, C. Liu, X. Wang, A phase field approach in the numerical study of the elastic bending energy for vesicle membranes. J. Comput. Phys. **198**, 450–468 (2004)
140. R.A. Sauer, T.X. Duong, K.K. Mandadapu, D.J. Steigmann, A stabilized finite element formulation for liquid shells and its application to lipid bilayers. J. Comput. Phys. **330**, 436–466 (2017)
141. S. Aland, S. Egerer, J. Lowengrub, A. Voigt, Diffuse interface models of locally inextensible vesicles in a viscous fluid. J. Comput. Phys. **277**, 32–47 (2014)
142. H. Noguchi, G. Gompper, Dynamics of fluid vesicles in shear flow: effect of the membrane viscosity and thermal fluctuations. Phys. Rev. E **72**, 011901 (2005)
143. P.B. Canham, The minimum energy of bending as a possible explanation of the biconcave shape of the human red blood cell. J. Theoret. Biol. **26**, 61–81 (1970)
144. M. Deserno, Fluid lipid membranes: from differential geometry to curvature stresses. Chem. Phys. Lipids **185**, 11–45 (2015)
145. G. Gompper, D.M. Kroll, Random surface discretizations and the renormalization of the bending rigidity. J. Phys. I France **6**, 1305–1320 (1996)
146. F. Jülicher, The morphology of vesicles of higher topological genus: conformal degeneracy and conformal modes. J. Phys. II France **6**, 1797–1824 (1996)
147. K. Tsubota, Short note on the bending models for a membrane in capsule mechanics: comparison between continuum and discrete models. J. Comput. Phys. **277**, 320–328 (2014)
148. A. Guckenberger, M.P. Schraml, P.G. Chen, M. Leonetti, S. Gekle, On the bending algorithms for soft objects in flows. Comput. Phys. Commun. **207**, 1–23 (2016)
149. A. Guckenberger, S. Gekle, Theory and algorithms to compute Helfrich bending forces: a review. J. Phys.: Condens. Matter **29**, 203001 (2017)
150. X. Bian, S. Litvinov, P. Koumoutsakos, Bending models of lipid bilayer membranes: spontaneous curvature and area-difference elasticity. Comput. Methods Appl. Mech. Eng. **359**, 112758 (2020)
151. C. Zhu, C.T. Lee, P. Rangamani, Mem3DG: modeling membrane mechanochemical dynamics in 3D using discrete differential geometry. Biophys. Rep. **2**, 100062 (2022)
152. H. Noguchi, G. Gompper, Fluid vesicles with viscous membranes in shear flow. Phys. Rev. Lett. **93**, 258102 (2004)
153. M.P. Allen, D.J. Tildesley, *Computer simulation of liquids* (Clarendon Press, New York, 1991)

154. S. Succi, *The Lattice Boltzmann equation for fluid dynamics and beyond* (Oxford University Press, Oxford, 2001)
155. J. F. Wendt, editor. *Computational Fluid Dynamics*. Springer, Berlin, 3rd edition, 2009
156. I.V. Pivkin, B. Caswell, G.E. Karniadakis, Dissipative particle dynamics, in *Reviews in Computational Chemistry*, vol. 27, ed. by K.B. Lipkowitz (John Wiley & Sons Inc, Hoboken, 2011), pp.85–110
157. M. Ellero, P. Español, Everything you always wanted to know about SDPD* (*but were afraid to ask). Appl. Math. Mech. **39**, 103–124 (2018)
158. G. Gompper, T. Ihle, D.M. Kroll, R.G. Winkler, Multi-particle collision dynamics: a particle-based mesoscale simulation approach to the hydrodynamics of complex fluids. Adv. Polym. Sci. **221**, 1–87 (2009)
159. J.J. Monaghan, Smoothed particle hydrodynamics. Rep. Prog. Phys. **68**, 1703–1759 (2005)
160. C.S. Peskin, The immersed boundary method. Acta Numer. **11**, 479–517 (2002)
161. Y. Liu, W.K. Liu, Rheology of red blood cell aggregation by computer simulation. J. Comput. Phys. **220**, 139–154 (2006)
162. P. Ahlrichs, B. Dünweg, Simulation of a single polymer chain in solution by combining lattice Boltzmann and molecular dynamics. J. Chem. Phys. **111**, 8225–8239 (1999)
163. T.R. Powers, Dynamics of filaments and membranes in a viscous fluid. Rev. Mod. Phys. **82**, 1607–1631 (2010)
164. D.J. Steigmann, Fluid films with curvature elasticity. Arch. Ration. Mech. Anal. **150**, 127–152 (1999)
165. C. Pozrikidis, Interfacial dynamics for Stokes flow. J. Comput. Phys. **169**, 250–301 (2001)
166. P. Schwille, J. Spatz, K. Landfester, E. Bodenschatz, S. Herminghaus, V. Sourjik, T.J. Erb, P. Bastiaens, R. Lipowsky, A. Hyman, P. Dabrock, J.-C. Baret, T. Vidakovic-Koch, P. Bieling, R. Dimova, H. Mutschler, T. Robinson, T.-Y.D. Tang, S. Wegner, K. Sundmacher, MaxSynBio: avenues towards creating cells from the bottom up. Angew. Chem. Int. Ed. **57**, 13382–13392 (2018)
167. D. Needleman, Z. Dogic, Active matter at the interface between materials science and cell biology. Nat. Rev. Mater. **2**, 17048 (2017)
168. K. Weirich, K.L. Dasbiswas, T.A. Witten, S. Vaikuntanathan, M.L. Gardel, Self-organizing motors divide active liquid droplets. Proc. Natl. Acad. Sci. USA **116**, 11125–11130 (2019)
169. A.P. Berke, L. Turner, H.C. Berg, E. Lauga, Hydrodynamic attraction of swimming microorganisms by surfaces. Phys. Rev. Lett. **101**, 038102 (2008)
170. G. Li, J.X. Tang, Accumulation of microswimmers near a surface mediated by collision and rotational Brownian motion. Phys. Rev. Lett. **103**, 078101 (2009)
171. J. Elgeti, G. Gompper, Wall accumulation of self-propelled spheres. Europhys. Lett. **101**, 48003 (2013)
172. S. Dasgupta, T. Auth, G. Gompper, Shape and orientation matter for the cellular uptake of nonspherical particles. Nano Lett. **14**, 687–693 (2014)
173. A.H. Bahrami, M. Raatz, J. Agudo-Canalejo, R. Michel, E.M. Curtis, C.K. Hall, M. Gradzielski, R. Lipowsky, T.R. Weikl, Wrapping of nanoparticles by membranes. Adv. Colloid Interface Sci. **208**, 214–224 (2014)
174. A. Šarić, A. Cacciuto, Mechanism of membrane tube formation induced by adhesive nanocomponents. Phys. Rev. Lett. **109**, 188101 (2012)
175. M. Raatz, R. Lipowsky, T.R. Weikl, Cooperative wrapping of nanoparticles by membrane tubes. Soft Matter **10**, 3570–3577 (2014)
176. Q. Yu, S. Othman, S. Dasgupta, T. Auth, G. Gompper, Nanoparticle wrapping at small non-spherical vesicles: curvatures at play. Nanoscale **10**, 6445–6458 (2018)
177. A.H. Bahrami, R. Lipowsky, T.R. Weikl, The role of membrane curvature for the wrapping of nanoparticles. Soft Matter **12**, 581–587 (2016)
178. A. Šarić, A. Cacciuto, Fluid membranes can drive linear aggregation of adsorbed spherical nanoparticles. Phys. Rev. Lett. **108**, 118101 (2012)
179. S. Dasgupta, T. Auth, G. Gompper, Wrapping of ellipsoidal nano-particles by fluid membranes. Soft Matter **9**, 5473–5482 (2013)
180. J. McCullough, A.K. Clippinger, N. Talledge, M.L. Skowyra, M.G. Saunders, T.V. Naismith, L.A. Colf, P. Afonine, C. Arthur, W.I. Sundquist, P.I. Hanson, A. Frost, Structure and membrane remodeling activity of ESCRT-III helical polymers. Science **350**, 1548–1551 (2015)
181. J.G. Carlton, J. Martin-Serrano, Parallels between cytokinesis and retroviral budding: a role for the ESCRT machinery. Science **316**, 1908–1912 (2007)
182. M.A.Y. Adell, G.F. Vogel, M. Pakdel, M. Müller, H. Lindner, M.W. Hess, D. Teis, Coordinated binding of Vps4 to ESCRT-III drives membrane neck constriction during MVB vesicle formation. J. Cell Biol. **205**, 33–49 (2014)
183. P.D. Bieniasz, Late budding domains and host proteins in enveloped virus release. Virology **344**, 55–63 (2006)
184. W.M. Henne, N.J. Buchkovich, Y. Zhao, S.D. Emr, The endosomal sorting complex ESCRT-II mediates the assembly and architecture of ESCRT-III helices. Cell **151**, 356–371 (2012)
185. N. Chiaruttini, A. Roux, Dynamic and elastic shape transitions in curved ESCRT-III filaments. Curr. Opin. Cell Biol. **47**, 126–135 (2017)
186. W. Pezeshkian, J.H. Ipsen, Mesoscale simulation of biomembranes with FreeDTS. Nat. Comm. **15**, 548 (2024)
187. G. Kumar, N. Ramakrishnan, A. Sain, Tubulation pattern of membrane vesicles coated with biofilaments. Phys. Rev. E **99**, 022414 (2019)
188. R. Lipowsky, Spontaneous tubulation of membranes and vesicles reveals membrane tension generated by spontaneous curvature. Faraday Discuss. **161**, 305–331 (2013)

189. M. Goulian, R. Bruinsma, P. Pincus, Long-range forces in heterogeneous fluid membranes. Europhys. Lett. **22**, 145–150 (1993)
190. P.G. Dommersnes, J.-B. Fournier, N-body study of anisotropic membrane inclusions: membrane mediated interactions and ordered aggregation. Eur. Phys. J. B **12**, 9–12 (1999)
191. H.-K. Lin, R. Zandi, U. Mohideen, L.P. Pryadko, Fluctuation-induced forces between inclusions in a fluid membrane under tension. Phys. Rev. Lett **107**, 228104 (2011)
192. A.H. Bahrami, T.R. Weikl, Curvature-mediated assembly of Janus nanoparticles on membrane vesicles. Nano Lett. **18**, 1259–1263 (2018)
193. J. Midya, T. Auth, G. Gompper, Membrane-mediated interactions between nonspherical elastic particles. ACS Nano **17**, 1935–1945 (2023)
194. N. Ramakrishnan, P.B.S. Kumar, R. Radhakrishnan, Mesoscale computational studies of membrane bilayer remodeling by curvature-inducing proteins. Phys. Rep. **543**, 1–60 (2014)
195. G. Kumar, A. Srivastava, Membrane remodeling due to a mixture of multiple types of curvature proteins. J. Chem. Theory Comput. **18**, 5659–5671 (2022)
196. Y.-H. Tang, L. Lu, H. Li, C. Evangelinos, L. Grinberg, V. Sachdeva, G.E. Karniadakis, OpenRBC: a fast simulator of red blood cells at protein resolution. Biophys. J. **112**, 2030–2037 (2017)
197. D.A. Fedosov, B. Caswell, G.E. Karniadakis, Systematic coarse-graining of spectrin-level red blood cell models. Comput. Meth. Appl. Mech. Eng. **199**, 1937–1948 (2010)
198. C. Pozrikidis, Numerical simulation of cell motion in tube flow. Ann. Biomed. Eng. **33**, 165–178 (2005)
199. S. Mendez, E. Gibaud, F. Nicoud, An unstructured solver for simulations of deformable particles in flows at arbitrary Reynolds numbers. J. Comput. Phys. **256**, 465–483 (2014)
200. J. Sigüenza, S. Mendez, D. Ambard, F. Dubois, F. Jourdan, R. Mozul, F. Nicoud, Validation of an immersed thick boundary method for simulating fluid-structure interactions of deformable membranes. J. Comput. Phys. **322**, 723–746 (2016)
201. T. Ye, N. Phan-Thien, B.C. Khoo, C.T. Lim, Dissipative particle dynamics simulations of deformation and aggregation of healthy and diseased red blood cells in a tube flow. Phys. Fluids **26**, 111902 (2014)
202. T. Ye, N. Phan-Thien, C.T. Lim, Y. Li, Red blood cell motion and deformation in a curved microvessel. J. Biomech. **65**, 12–22 (2017)
203. J. Mauer, S. Mendez, L. Lanotte, F. Nicoud, M. Abkarian, G. Gompper, D.A. Fedosov, Flow-induced transitions of red blood cell shapes under shear. Phys. Rev. Lett. **121**, 118103 (2018)
204. J.L. McWhirter, H. Noguchi, G. Gompper, Ordering and arrangement of deformed red blood cells in flow through microcapillaries. New J. Phys. **14**, 085026 (2012)
205. D.A. Fedosov, B. Caswell, A.S. Popel, G.E. Karniadakis, Blood flow and cell-free layer in microvessels. Microcirculation **17**, 615–628 (2010)
206. D.A. Fedosov, W. Pan, B. Caswell, G. Gompper, G.E. Karniadakis, Predicting human blood viscosity in silico. Proc. Natl. Acad. Sci. USA **108**, 11772–11777 (2011)
207. D. Katanov, G. Gompper, D.A. Fedosov, Microvascular blood flow resistance: role of red blood cell migration and dispersion. Microvasc. Res. **99**, 57–66 (2015)
208. W. Chien, G. Gompper, D.A. Fedosov, Effect of cytosol viscosity on the flow behavior of red blood cell suspensions in microvessels. Microcirculation **28**, e12668 (2021)
209. R. Skalak, A. Tozeren, R.P. Zarda, S. Chien, Strain energy function of red blood cell membranes. Biophys. J. **13**, 245–264 (1973)
210. D. Barthés-Biesel, J.M. Rallison, The time-dependent deformation of a capsule freely suspended in a linear shear flow. J. Fluid Mech. **113**, 251–267 (1981)
211. C. Pozrikidis, Axisymmetric motion of a file of red blood cells through capillaries. Phys. Fluids **17**, 031503 (2005)
212. J.P. Mills, L. Qie, M. Dao, C.T. Lim, S. Suresh, Nonlinear elastic and viscoelastic deformation of the human red blood cell with optical tweezers. Mech. Chem. Biosystems **1**, 169–180 (2004)
213. D. Barthés-Biesel, A. Diaz, E. Dhenin, Effect of constitutive laws for two-dimensional membranes on flow-induced capsule deformation. J. Fluid Mech. **460**, 211–222 (2002)
214. P. Bagchi, R.M. Kalluri, Rheology of a dilute suspension of liquid-filled elastic capsules. Phys. Rev. E **81**, 056320 (2010)
215. E. Foessel, J. Walter, A.-V. Salsac, D. Barthés-Biesel, Influence of internal viscosity on the large deformation and buckling of a spherical capsule in a simple shear flow. J. Fluid Mech. **672**, 477–486 (2011)
216. E. Lac, D. Barthés-Biesel, Deformation of a capsule in simple shear flow: effect of membrane prestress. Phys. Fluids **17**, 072105 (2005)
217. T. Omori, T. Ishikawa, D. Barthés-Biesel, A.-V. Salsac, Y. Imai, T. Yamaguchi, Tension of red blood cell membrane in simple shear flow. Phys. Rev. E **86**, 056321 (2012)
218. A. Yazdani, P. Bagchi, Influence of membrane viscosity on capsule dynamics in shear flow. J. Fluid Mech. **718**, 569–595 (2013)
219. Z. Wang, Y. Sui, P.D.M. Spelt, W. Wang, Three-dimensional dynamics of oblate and prolate capsules in shear flow. Phys. Rev. E **88**, 053021 (2013)
220. Y. Sui, Y.T. Chew, P. Roy, Y.P. Cheng, H.T. Low, Dynamic motion of red blood cells in simple shear flow. Phys. Fluids **20**, 112106 (2008)

221. S. Mendez, M. Abkarian, In-plane elasticity controls the full dynamics of red blood cells in shear flow. Phys. Rev. Fluids **3**, 101101 (2018)
222. S.K. Doddi, P. Bagchi, Lateral migration of a capsule in a plane Poiseuille flow in a channel. Int. J. Multiphase Flow **34**, 966–986 (2008)
223. C. Wang, J. Li, L. Zhao, P. Qian, Shape transformations of red blood cells in the capillary and their possible connections to oxygen transportation. J. Biol. Phys. **48**, 79–92 (2022)
224. M. Gross, T. Krüger, F. Varnik, Rheology of dense suspensions of elastic capsules: normal stresses, yield stress, jamming and confinement effects. Soft Matter **10**, 4360–4372 (2014)
225. M. Mehrabadi, D.N. Ku, C.K. Aidun, Effects of shear rate, confinement, particle parameters on margination in blood flow. Phys. Rev. E **93**, 023109 (2016)
226. K. Vahidkhah, P. Balogh, P. Bagchi, Flow of red blood cells in stenosed microvessels. Sci. Rep. **6**, 28194 (2016)
227. P. Balogh, P. Bagchi, A computational approach to modeling cellular-scale blood flow in complex geometry. J. Comput. Phys. **334**, 280–307 (2017)
228. P. Balogh, P. Bagchi, Direct numerical simulation of cellular-scale blood flow in 3D microvascular networks. Biophys. J. **113**, 2815–2826 (2017)
229. Q. Zhou, J. Fidalgo, M.O. Bernabeu, M.S.N. Oliveira, T. Krüger, Emergent cell-free layer asymmetry and biased haematocrit partition in a biomimetic vascular network of successive bifurcations. Soft Matter **17**, 3619–3633 (2021)
230. T. Browicz, Further observation of motion phenomena on red blood cells in pathological states. Zbl. Med. Wiss. **28**, 625 (1890)
231. J. Evans, W. Gratzer, N. Mohandas, K. Parker, J. Sleep, Fluctuations of the red blood cell membrane: relation to mechanical properties and lack of ATP dependence. Biophys. J. **94**, 4134–4144 (2008)
232. Y.Z. Yoon, J. Kotar, A.T. Brown, P. Cicuta, Red blood cell dynamics: from spontaneous fluctuations to non-linear response. Soft Matter **7**, 2042–2051 (2011)
233. R. Rodríguez-García, I. López-Montero, M. Mell, G. Egea, N.S. Gov, F. Monroy, Direct cytoskeleton forces cause membrane softening in red blood cells. Biophys. J. **108**, 2794–2806 (2015)
234. N.S. Gov, S.A. Safran, Red blood cell membrane fluctuations and shape controlled by ATP-induced cytoskeletal defects. Biophys. J. **88**, 1859–1874 (2005)
235. N.S. Gov, Active elastic network: cytoskeleton of the red blood cell. Phys. Rev. E **75**, 011921 (2007)
236. J.-B. Manneville, P. Bassereau, D. Lévy, J. Prost, Activity of transmembrane proteins induces magnification of shape fluctuations of lipid membranes. Phys. Rev. Lett. **82**, 4356–4359 (1999)
237. S. Ramaswamy, J. Toner, J. Prost, Nonequilibrium fluctuations, traveling waves, instabilities in active membranes. Phys. Rev. Lett. **84**, 3494–3497 (2000)
238. L.H. Miller, D.I. Baruch, K. Marsh, O.K. Doumbo, The pathogenic basis of malaria. Nature **415**, 673–679 (2002)
239. M. Koch, J. Baum, The mechanics of malaria parasite invasion of the human erythrocyte - towards a reassessment of the host cell contribution. Cell. Microbiol. **18**, 319–329 (2016)
240. K. Yahata, M. Treeck, R. Culleton, T.-W. Gilberger, O. Kaneko, Time-lapse imaging of red blood cell invasion by the rodent malaria parasite Plasmodium yoelii. PLoS ONE **7**, e50780 (2012)
241. G.A. Barabino, M.O. Platt, D.K. Kaul, Sickle cell biomechanics. Annu. Rev. Biomed. Eng. **12**, 345–367 (2010)
242. W. Pezeshkian, S.J. Marrink, Simulating realistic membrane shapes. Curr. Opin. Cell Biol. **71**, 103–111 (2021)
243. W. Pezeshkian, M. König, T.A. Wassenaar, S.J. Marrink, Backmapping triangulated surfaces to coarse-grained membrane models. Nat. Comm. **11**, 2296 (2020)
244. M. Sadeghi, F. Noé, Large-scale simulation of biomembranes incorporating realistic kinetics into coarse-grained models. Nat. Comm. **11**, 2951 (2020)
245. C.M. Elliott, B. Stinner, C. Venkataraman, Modelling cell motility and chemotaxis with evolving surface finite elements. J. R. Soc. Interface **9**, 3027–3044 (2012)
246. H. Berthoumieux, J.-L. Maître, C.-P. Heisenberg, E.K. Paluch, F. Jülicher, G. Salbreux, Active elastic thin shell theory for cellular deformations. New J. Phys. **16**, 065005 (2014)
247. A. Mietke, F. Jülicher, I.F. Sbalzarini, Self-organized shape dynamics of active surfaces. Proc. Natl. Acad. Sci. USA **116**, 29–34 (2019)
248. H. Li, G. Lykotrafitis, Erythrocyte membrane model with explicit description of the lipid bilayer and the spectrin network. Biophys. J. **107**, 642–653 (2014)
249. Z. Peng, X. Li, I.V. Pivkin, M. Dao, G.E. Karniadakis, S. Suresh, Lipid bilayer and cytoskeletal interactions in a red blood cell. Proc. Natl. Acad. Sci. USA **110**, 13356–13361 (2013)
250. H. Ni, G.A. Papoian, Membrane-MEDYAN: simulating deformable vesicles containing complex cytoskeletal networks. J. Phys. Chem. B **125**, 10710–10719 (2021)
251. N. Tamemoto, H. Noguchi, Reaction-diffusion waves coupled with membrane curvature. Soft Matter **17**, 6589–6596 (2021)